

## Smoke transport by sheared winds

Javier Trelles†, Kevin B McGrattan and Howard R Baum

National Institute of Standards and Technology, Gaithersburg, MD 20899, USA

Received 2 September 1998

**Abstract.** The effect that the wind's vertical variation has on fire plume behaviour is investigated. A parabolized set of governing equations are discretized using finite differences to arrive at the numerical model. Lagrangian particles are used to visualize the flow, account for atmospheric fluctuations and determine the smoke concentration field. A parametric study based on varying the wind lapse rate is performed. Four cases from actual soundings are analysed with both the actual and an averaged constant wind. The results suggest that an increasing wind profile suppresses plume dynamics, leading to decreased plume rise heights.

### Nomenclature

$c_p$	Specific heat coefficient at constant pressure ( $\text{J kg}^{-1} \text{K}^{-1}$ )
$f$	Stretching factor
$g$	Acceleration of gravity ( $9.81 \text{ m s}^{-2}$ )
$\mathcal{H}$	Total head (Pa)
$k$	Coefficient of thermal conductivity ( $\text{W m}^{-1} \text{K}^{-1}$ )
$L$	Characteristic length (m)
$M$	Total particulate mass flow rate ( $\text{kg s}^{-1}$ )
$N_0^2$	Square of the Brunt–Väisälä frequency = $-(g/\rho_0)(d\rho_0/dz)$ or $(g/T_0)(dT_0/dz + g/c_p)$ ( $\text{s}^{-2}$ )
$n$	Total number of particles in the plume
$Pr$	Turbulent Prandtl number ( $\mu c_p/k$ )
$p$	Pressure (Pa)
$Q$	Total heat release rate (W)
$\dot{q}$	Heat release rate per unit volume ( $\text{W m}^{-3}$ )
$\mathcal{R}$	Universal gas constant ( $\text{J kg}^{-1} \text{K}^{-1}$ )
$Re$	Turbulent Reynolds number ( $f^2 \rho V L/\mu$ )
$T$	Temperature (K)
$t$	Time (s)
$U_0$	Ambient wind ( $\text{m s}^{-1}$ )
$\mathbf{u}$	Velocity vector in the $y$ - $z$ -plane ( $v, w$ ) ( $\text{m s}^{-1}$ )
$u$	$x$ -component of the velocity ( $\text{m s}^{-1}$ )
$V$	Characteristic velocity of the air in the crosswind plane ( $\text{m s}^{-1}$ )
$v$	$y$ -component of the velocity ( $\text{m s}^{-1}$ )
$w$	$z$ -component of the velocity ( $\text{m s}^{-1}$ )

† Present address: Hughes Associates, Inc., 3610 Commerce Dr., Suite 817, Baltimore, MD 21227-1652, USA.

$\mathbf{x}$	Position vector ( $x, y, z$ ) (m)
$x$	First Cartesian coordinate (m)
$y$	Second Cartesian coordinate (m)
$z$	Third Cartesian coordinate (m)
$\nabla$	Gradient in the $y$ - $z$ -plane ( $\text{m}^{-1}$ )
$\beta_j$	Plume cross sectional half-width in the $j$ -direction (m)
$\theta$	Potential temperature = $T(p_\infty/p)^{R/c_p}$ (K)
$\mu$	Coefficient of viscosity ( $\text{kg m}^{-1} \text{s}^{-1}$ )
$\rho$	Density ( $\text{kg m}^{-3}$ )
$\rho_p$	Smoke concentration ( $\mu\text{g m}^{-3}$ )
$\sigma_\theta, \sigma_\phi$	Turbulent fluctuations in the $y$ - and $z$ -directions, respectively.

#### Subscripts

0	Quantity that only depends on $z$
$\infty$	Ground level, ambient condition
$p$	Referring to particulate quantities

#### Superscripts

*	Dimensionless variable
$\sim$	Perturbation quantity

## 1. Introduction

As a medium for air pollution, fire plumes, whether from accidental urban or forest fires or from intentional fires, such as those used to consume marine oil spills, are distinguished from most other air-borne emission sources by the strong buoyancy forces they generate. These forces can cause the plume to penetrate far higher into the atmosphere than most municipal plume sources. Since the fire plume can rise through several hundred metres in very little time, it is desirable to incorporate into any model as many features prevalent in the atmosphere for that altitude interval as possible. The following research applies the low-Mach-number equations for thermally driven, buoyant flows as laid down in [1] to the problem of large-scale fire plumes in the presence of winds which vary in the vertical direction. The analysis presented here is based on extensions of the numerical work in [2–5] for a uniform ambient wind. The same governing equations were solved using random vortex methods by Zhang, Ghoniem and co-workers, [6–9] who strongly emphasized vortex dynamics studies but have not extended their approach to support non-uniform ambient wind profiles. The approach chosen here is to use finite differences for the methodology and to focus on the particulate dynamics of plumes being advected by an atmospheric wind which varies with elevation.

The goals of the present effort are to extend the capabilities of the existing plume model [2–5] so that it can handle the data distributed by the National Oceanic and Atmospheric Administration (NOAA) [11, 10] without having to average the wind profiles therein over height and then to investigate the outcome of the wind's vertical variability on smoke transport. The paper is organized as follows. First the assumptions behind this model are stated and the resulting governing equations are presented. Scaling appropriate for a variable wind profile is introduced. The derived characteristic quantities are used to non-dimensionalize the governing equations, preparing the mathematical model for numerical integration. The techniques used to solve the equations are discussed along with the associated error estimates. Four examples

demonstrate the smoke transport consequences of interesting wind profiles taken directly from the NOAA database [11].

## 2. Mathematical model

The steady state equations that describe the plume dynamics are based on the Boussinesq form of the Navier–Stokes equations. The prevailing windward ( $x$ ) component of the velocity is replaced by an ambient wind which only varies in the vertical ( $z$ ) direction. The crosswind components ( $y, z$ ) are subject to slight variations characteristic of atmospheric turbulence. After these simplifications, described in more detail below, the three-dimensional, steady-state system of equations becomes equivalent to a two-dimensional, time-dependent system. It can now be characterized as an initial value problem in which the initial solution is prescribed in a plane perpendicular to the direction of the prevailing wind. This initial plane is taken to be a few fire diameters downwind of the fire. The simplified equations resulting from these assumptions can be solved in sufficient detail to resolve the plume rise down to a length scale in the range of 10 m within a domain several kilometres on a side. This is sufficient to capture the entrainment of air into the smoke plume and to describe the plume rise over flat terrain. This domain is comparable to that used for a single cell in a regional meteorological simulation.

The Boussinesq approximation assumes that, several diameters downstream of the fire, the induced temperature and density differences are a small fraction of their ambient ground-level values [1]. The pressure,  $p$ , temperature,  $T$ , and density,  $\rho$ , are divided into a vertically varying term, subscripted with a 0, and fire-induced perturbation terms, denoted by a tilde. The ambient pressure,  $p_0$ , and density,  $\rho_0$ , are related through the hydrostatic condition

$$\frac{dp_0}{dz} = -\rho_0 g \quad (1)$$

where  $g$  is the acceleration of gravity, and the temperature and density perturbations can be related through the equation of state taken in the small-disturbance, low-Mach-number form appropriate to this problem

$$(\rho - \rho_0)/\rho_0 = -(T - T_0)/T_0. \quad (2)$$

The most important consequence of this form of the equations is that the convective derivative of pressure in the energy equation is approximated as  $dp_0/dt \approx w dp_0/dz$ . This simplification and equation (2) eliminate acoustic waves from the solution. The prevailing wind is aligned with the positive  $x$ -axis and the streamwise diffusion is ignored. The crosswind velocity components,  $(v, w)$ , lie in the  $y$ - $z$ -plane normal to the direction ( $x$ ) in which the ambient wind,  $U_0(z)$ , flows. The simplified equations that result are:

conservation of mass

$$\frac{\partial v}{\partial y} + \frac{\partial w}{\partial z} = 0 \quad (3)$$

conservation of momentum

$$\rho_0 \left( U_0(z) \frac{\partial v}{\partial x} + v \frac{\partial v}{\partial y} + w \frac{\partial v}{\partial z} \right) + \frac{\partial \tilde{p}}{\partial y} = \mu \left( \frac{\partial^2 v}{\partial y^2} + \frac{\partial^2 v}{\partial z^2} \right) \quad (4)$$

$$\rho_0 \left( U_0(z) \frac{\partial w}{\partial x} + v \frac{\partial w}{\partial y} + w \frac{\partial w}{\partial z} \right) + \frac{\partial \tilde{p}}{\partial z} + \tilde{\rho} g = \mu \left( \frac{\partial^2 w}{\partial y^2} + \frac{\partial^2 w}{\partial z^2} \right) \quad (5)$$

conservation of energy

$$\rho_0 c_p \left( U_0(z) \frac{\partial \tilde{T}}{\partial x} + v \frac{\partial \tilde{T}}{\partial y} + w \frac{\partial \tilde{T}}{\partial z} \right) - \left( \frac{dp_0}{dz} - \rho_0 c_p \frac{dT_0}{dz} \right) w = k \left( \frac{\partial^2 \tilde{T}}{\partial y^2} + \frac{\partial^2 \tilde{T}}{\partial z^2} \right). \quad (6)$$

The coefficients of eddy viscosity  $\mu$  and eddy thermal conductivity  $k$  are constants in any given simulation whose size is dependent on the spatial resolution limit imposed by the computational grid.

The required information about the fires is the total *convective* heat release rate,  $Q$ , and the total particulate mass flow rate,  $M$ . The temperature distribution is initialized as a Gaussian centred at the plume's introduction point. It satisfies the integral

$$\int_{-\infty}^{\infty} \int_0^{\infty} \rho_{\infty} c_p U_0(z) \bar{T} dz dy = Q. \quad (7)$$

The particulate matter is considered as a passive scalar and thus has no effect on the hydrodynamic scaling or calculation.

The scaling of the governing equations is based on the net strength of the fires, the ground-level thermodynamics of the atmosphere and the maximum of the prevailing ambient wind,  $U_{\max} = \max\{U_0(z)\}$ . Scales in the  $x$ -direction differ from those in the  $y$ - $z$ -plane. The physical length scale in the  $y$ - $z$ -plane is given by

$$L = \left( \frac{Qg}{c_p T_{\infty} \rho_{\infty} U_{\max} N_{\infty}^2} \right)^{1/3} \quad (8)$$

where  $L$  is of the order of the plume rise height. The new quantity in equation (8) is the Brunt-Väisälä frequency, defined as  $N_0^2 = (g/\theta_0)(d\theta_0/dz) = (g/T_0)(dT_0/dz + g/c_p)$ .  $\theta = T(p_{\infty}/p)^{R/c_p}$  is the potential temperature. For all variables, the subscript  $\infty$  refers to the ground level, ambient quantity. The non-dimensional variables in the windward direction are

$$U_0^* = U_0/U_{\max} \quad \text{and} \quad x^* = (N_{\infty}/U_{\max})x. \quad (9)$$

The physical velocity scale of the air in the crosswind plane is given by

$$V = N_{\infty}L. \quad (10)$$

For this model to be feasible, the lower limit  $U_0(z) \geq V$  for all  $z$  is placed on the ambient wind profile. An adjustable scale factor,  $f$ , is used to ensure that the plumes do not rise out of the height of the physical domain,  $L$ . Now the computational length scale,  $fL$ , and velocity scale,  $fV$ , are used to define dimensionless crosswind spatial coordinates ( $y^*$ ,  $z^*$ ) and velocities ( $v^*$ ,  $w^*$ ) as follows:

$$(y, z) = fL(y^*, z^*) \quad \text{and} \quad (v, w) = fV(v^*, w^*). \quad (11)$$

The non-dimensional temperature perturbation,  $\tilde{T}^*$ , and pressure perturbation,  $\tilde{p}^*$ , are, respectively, defined as

$$\tilde{T} = \frac{fQ}{c_p \rho_{\infty} U_{\max} L^2} \tilde{T}^* \quad \text{and} \quad \tilde{p} = \rho_{\infty} f^2 V^2 \tilde{p}^*. \quad (12)$$

Finally, the turbulent Reynolds and Prandtl numbers, respectively, are

$$Re = (f^2 \rho_{\infty} V L) / \mu \quad \text{and} \quad Pr = (\mu c_p) / k. \quad (13)$$

Initially, the crosswind velocity components  $v$  and  $w$  are assumed to be zero since previous experience (see [3, 4]) has shown that the settling of particulate from the plume is insensitive to the initial velocity condition. Downwind, no-flux, free-slip boundary conditions are prescribed at the ground, consistent with the resolution limits of the calculation. The perturbation temperature is adiabatic at all boundaries. The perturbation pressure has zero normal derivative at the ground and zero value at all other boundaries.

The smoke concentration field is determined by transporting Lagrangian particles through the calculated velocity field and then distributing their locations and values onto the computational grid at each computational plane. The trajectories of the Lagrangian particles

used to represent the smoke particulate are randomly perturbed from their mean paths in order to mimic spatial and temporal fluctuations of the wind and the underlying turbulence. It is assumed that the background atmospheric wind field fluctuates by an angle  $\sigma_\theta$  in the  $y$ -direction and by an angle  $\sigma_\phi$  in the  $z$ -direction. The values  $(\sigma_\theta, \sigma_\phi) = (\pm 5^\circ, \pm 5^\circ)$  are used for the four cases in this investigation. The physics of atmospheric mixing, as applied in this instance, is identical to that presented in detail in a previous publication [3].

### 3. Numerical methods

Finite differences on a staggered grid are used to discretize the partial differential equations of motion. A second-order, modified Euler Runge–Kutta scheme with variable step size is used to advance the discretized field variables and to transport the particulate through the computed plume environment. The discretized versions of the governing equations are implemented numerically as in [3] with the exception that  $1/U_0^*(z^*)$  appears explicitly as a factor on all the terms except those entailing the partial derivative with respect to  $x^*$ . The greatest difference comes from the pressure update equation. By taking the divergence of the momentum equation in the vector-invariant form, a Poisson equation for the total head,  $\mathcal{H}^*$ , is obtained,

$$\frac{\partial^2 \mathcal{H}^*}{\partial y^{*2}} + U_0^* \frac{\partial}{\partial z^*} \left( \frac{1}{U_0^*} \frac{\partial \mathcal{H}^*}{\partial z^*} \right) = -U_0^* \nabla \cdot \mathbf{F}^* \quad (14)$$

where  $\mathcal{H}^* = |\mathbf{u}^*|^2/2 + \tilde{p}^*$  and  $\mathbf{F}^*$  contains all the convective and buoyancy terms. The discretized equation (14) is solved with a very efficient direct Poisson solver known as CRAYFISHPAK [12], which exploits the uniform gridding of the computational domain through the use of fast Fourier transforms (FFTs) [12], suitably modified to incorporate the  $z^*$  dependence of  $U_0^*$ . However, the boundary conditions for all the equations remain unchanged. Similarly, the numerical procedures for processing the Lagrangian particles are identical to those described previously in [3].

The accuracy of the Poisson solver is verified by solving equation (14) analytically for  $U_0^* = e^{-z^*}$ , the right-hand side is equal to a delta function, and with the same boundary conditions as those for the perturbation pressure. The same problem is solved with CRAYFISHPAK, where the delta function is replaced by a normalized spike. The two solutions, when compared, are found to be in agreement.

Numerical experiments are carried out in order to quantify the errors and costs associated with this method. For these experiments, a 500 MW fire producing smoke at  $2.5 \text{ kg s}^{-1}$  is used. 7000 Lagrangian particles are employed to track the smoke trajectory. The initial particle distribution in the  $y$ – $z$ -plane is circular with a diameter of 80 m, the atmosphere is linearly stratified at  $-5^\circ\text{C}$ ,  $f = 4$ , and the prevailing ambient wind increases exponentially from  $5 \text{ m s}^{-1}$  at the ground to  $10 \text{ m s}^{-1}$  at the top of the computational domain. The atmospheric dispersion angles are zero in both the  $y$ - and the  $z$ -directions.

To test the convergence of the computations, the perturbation temperature,  $\tilde{T}$ , is averaged over the cross section at each  $x$  location. Richardson extrapolation is applied to the curves corresponding with the two most refined grids. This best estimate is compared with the curve for the most refined grid, yielding a maximum error of 1.8% over the dynamic range of the integrated perturbation temperature. As was mentioned above, when the grid resolution is increased, the turbulent Reynolds number,  $Re$ , is increased so that, if  $\delta$  is the grid size,  $Re \delta^2$  is a fixed number of order unity.

The preceding calculations were done in double precision and proceeded up to  $x = 8 \text{ km}$  (i.e.  $x^* = 5$ ). The  $512 \times 128$  resolution case had  $Re = 20\,000$  and required 818 steps and 17.3 Mbytes of memory to run to completion in 7.1 min on an SGI workstation with the R10000

CPU. For  $256 \times 64$ ,  $Re = 5\,000\,280$  steps were taken and 9.6 Mbytes were used in 0.56 min on the same hardware. 142 steps were taken and 6.0 Mbytes were used in 6.5 s for the coarsest case of  $128 \times 32$  which had  $Re = 1250$ .

In addition to the exercises discussed above, parametric studies and investigations of idealized wind profiles were conducted. For the parametric studies, an exponentially increasing wind was chosen. Through a series of 22 runs, it was varied from a constant  $10\text{ m s}^{-1}$  to one where the ground level velocity was an order of magnitude less than the  $10\text{ m s}^{-1}$  at the top. The temperature was fixed at a linear rate of  $-5^\circ\text{C km}^{-1}$ . These runs established, among other things, that the greater the rate with which the velocity increased with height, the more stabilized the plume became. This effect will be more fully analysed in the next section. The

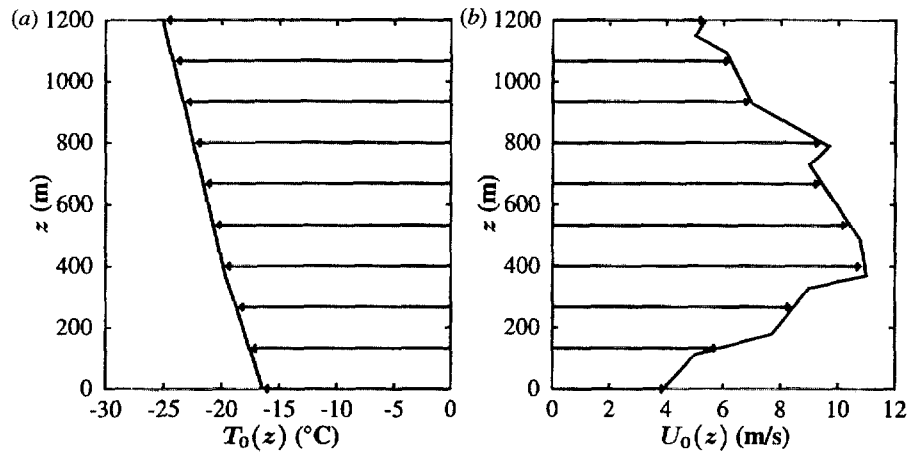


**Figure 1.** These two profiles resulted from a sounding taken in Fairbanks, Alaska, on November 7 1990, at 12:00 UTC which was catalogued in the NOAA database. The velocity profile is a good example of a complex function, but it also shares some similarities with the idealized planar jet profile. The temperature is nearly linear. (a) Stratification temperature profile; (b) ambient wind profile.

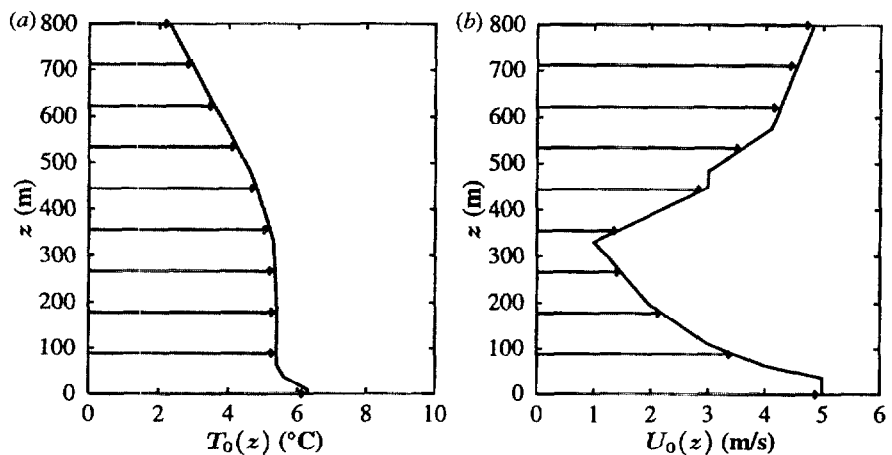


**Figure 2.** These two profiles resulted from a sounding taken in Anchorage, Alaska, on October 7 1990, at 0:00 UTC which was catalogued in the NOAA database. The velocity profile is planar wake-like in character. (a) Stratification temperature profile; (b) ambient wind profile.

idealized winds include shear layer, jet stream and gravity current profiles. The results from these investigations established that the vertical wind change can have pronounced effects on the plume dynamics and, furthermore, they motivated the choice of sounding files used in the following section.

#### 4. Results

In this section, the effects on smoke transport by four physically pertinent sheared wind profiles are investigated. The regional and seasonal meteorological data are provided by the NOAA [10, 11] sounding files. Each sounding typically covers an altitude range of several thousand metres. Care was taken by the tabulators to exclude data points characterized by unusually

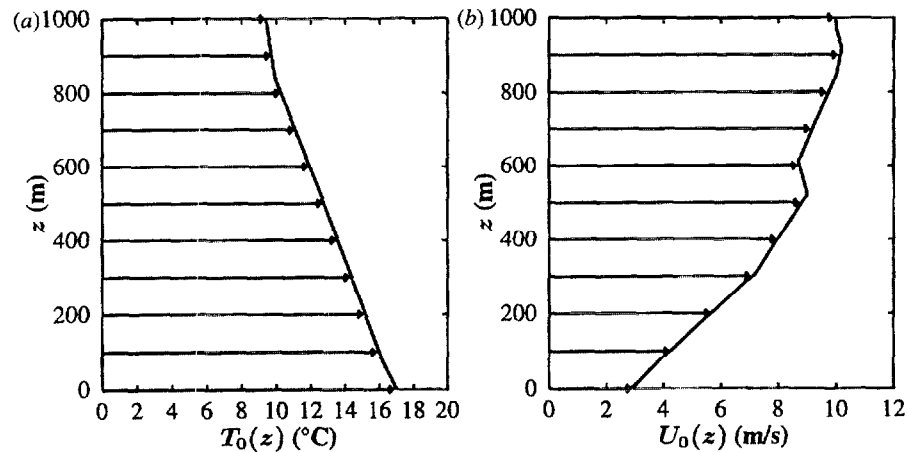


**Figure 3.** These two profiles resulted from a sounding taken in Oakland, California, on October 22 1991, at 12:00 UTC which was catalogued in the NOAA database. This wind profile is generally increasing with height. (a) Stratification temperature profile; (b) ambient wind profile.

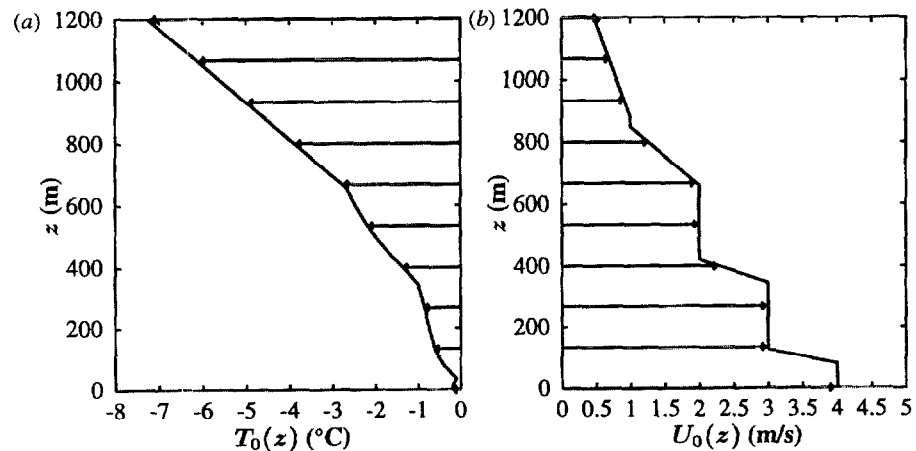


**Figure 4.** These two profiles resulted from a sounding taken in Anchorage, Alaska, on October 30 1990, at 12:00 UTC which was catalogued in the NOAA database. This wind profile is generally decreasing with height. (a) Stratification temperature profile; (b) ambient wind profile.

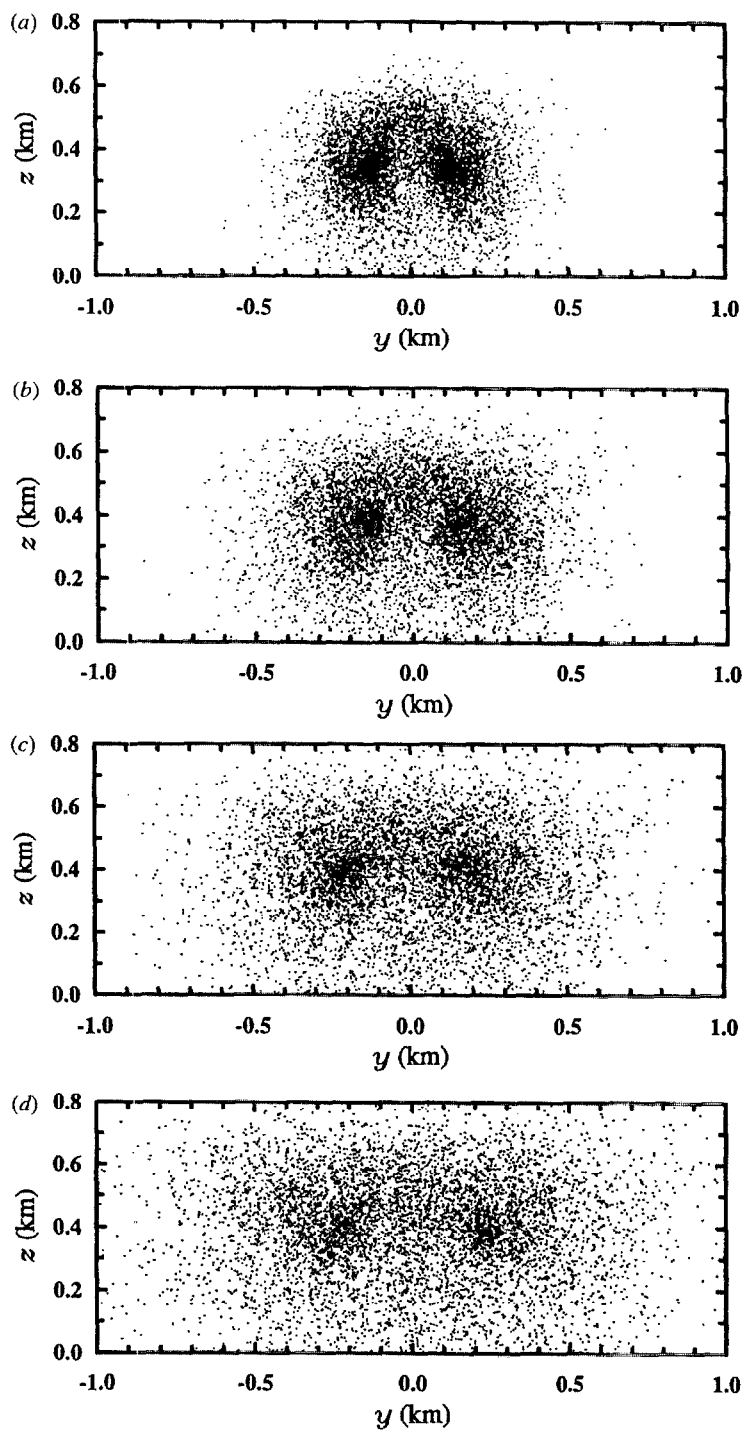


**Figure 5.** These four cross sections at  $x = (3, 4, 5, 6)$  km of the particulate locations, generated with atmospheric mixing of intensity  $(\pm 5^\circ, \pm 5^\circ)$  and the ambient conditions for Fairbanks, Alaska, on November 7 1990, at 12:00 UTC shown in figure 1, show that the fire's effect on the smoke is essentially gone by  $x = 6$  km. (a)  $x = 3$  km, (b)  $x = 4$  km, (c)  $x = 5$  km and (d)  $x = 6$  km.

high errors or resulting from equipment malfunctions. The result of these two facts is that the profiles reproduced here in figures 1–4 will seem sparse since this investigation only needs

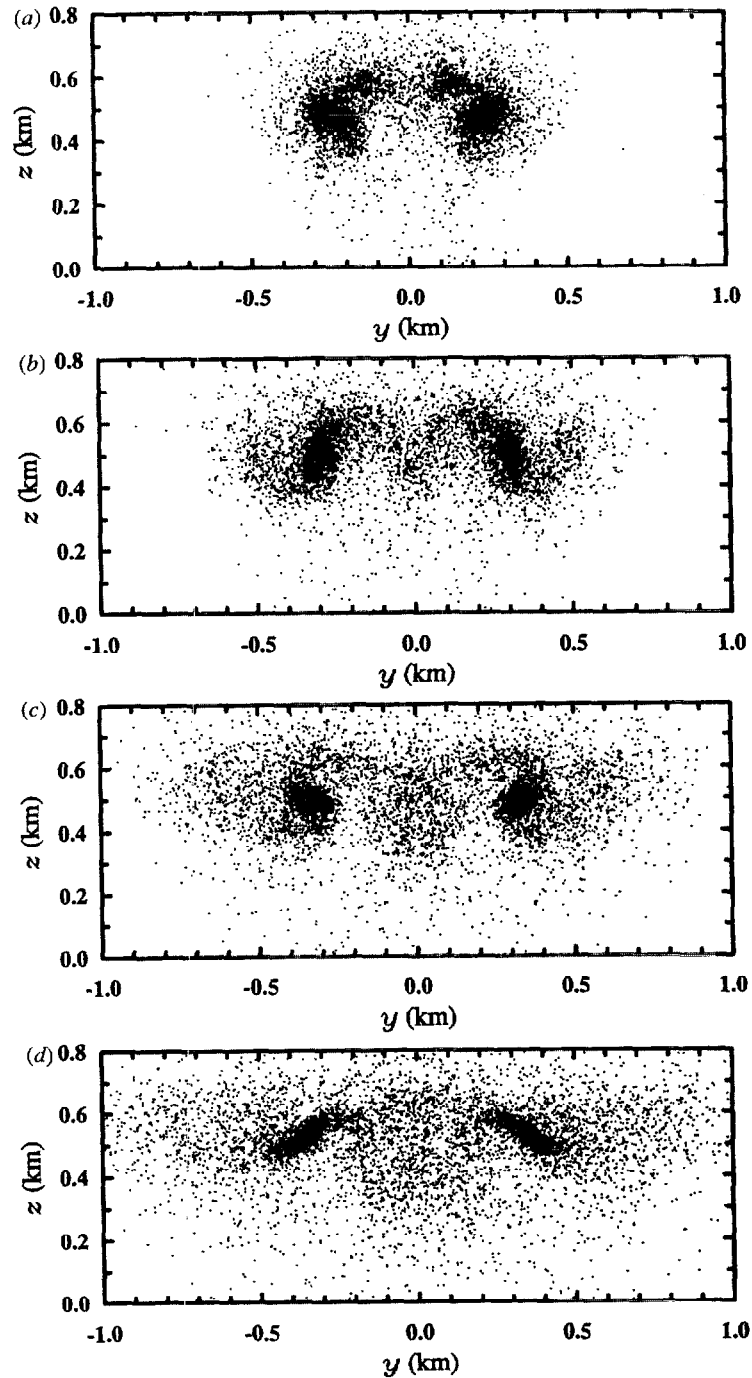


**Figure 6.** These four cross sections at  $x = (3, 4, 5, 6)$  km of the particulate locations, generated with atmospheric mixing of intensity  $(\pm 5^\circ, \pm 5^\circ)$ , the temperature sounding profile from Fairbanks, Alaska, on November 7 1990, at 12:00 UTC shown in figure 1(a), and a constant  $7.2 \text{ m s}^{-1}$  wind profile, show greater plume rise and stronger vortex dynamics than in figure 5. (a)  $x = 3$  km, (b)  $x = 4$  km, (c)  $x = 5$  km and (d)  $x = 6$  km.

meteorological information within about the 1000 m. However, spline interpolation is used to interpolate the profiles onto the grid which in turn helps to smooth out their inherent roughness.

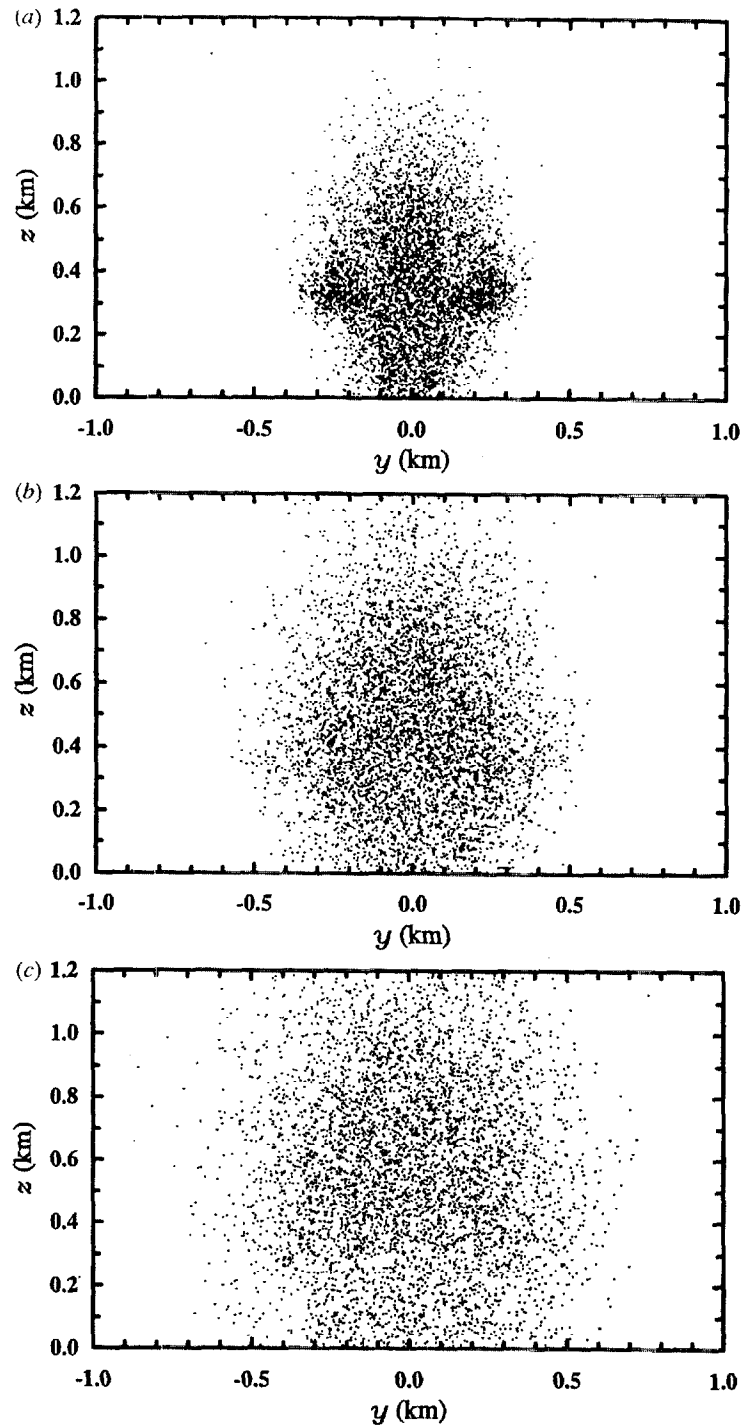


**Figure 7.** These four cross sections at  $x = (2, 3, 4, 5)$  km of the particulate locations were generated with atmospheric mixing of intensity ( $\pm 5^\circ, \pm 5^\circ$ ) and the ambient conditions for Anchorage, Alaska, on October 7 1990, at 0:00 UTC shown in figure 2. (a)  $x = 2$  km, (b)  $x = 3$  km, (c)  $x = 4$  km and (d)  $x = 5$  km.

The four choices presented here in figures 1–4 are based on physically interesting profiles. The subsequent results not only help to establish the important role played by the wind profile, but

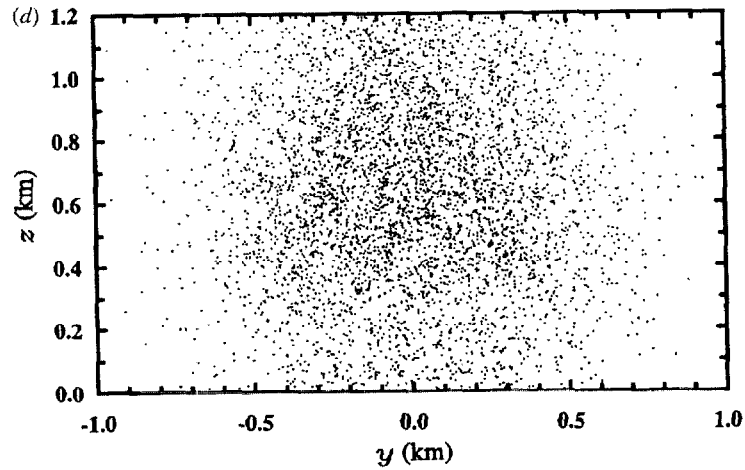
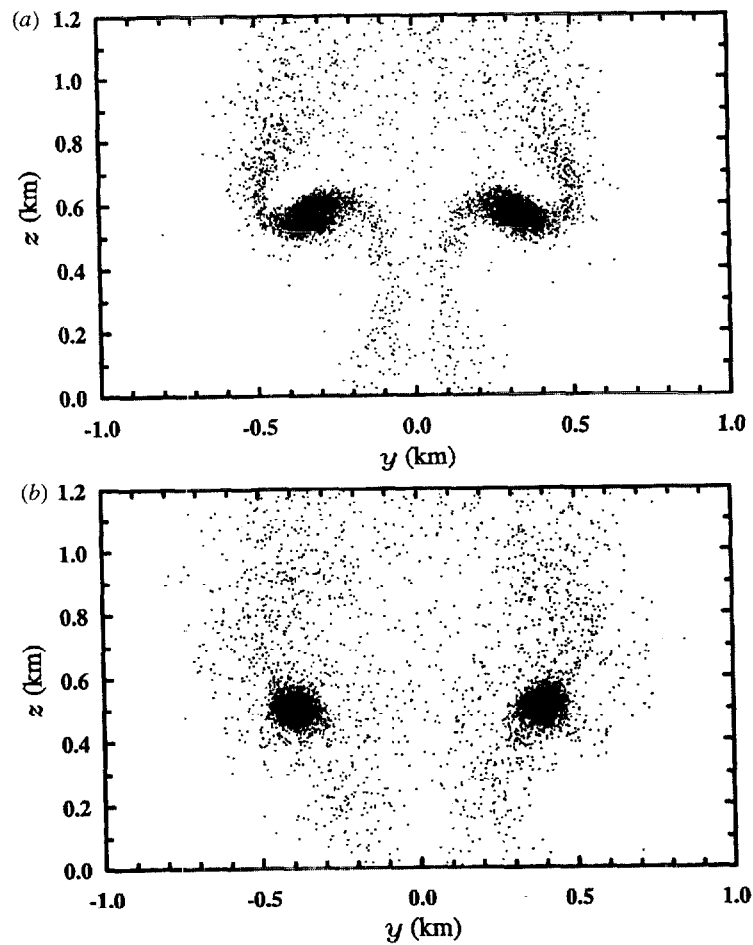


Figure 7. Continued.



**Figure 8.** These four cross sections at  $x = (2, 3, 4, 5)$  km of the particulate locations, generated with atmospheric mixing of intensity  $(\pm 5^\circ, \pm 5^\circ)$ , the temperature sounding profile for Anchorage, Alaska, on October 7 1990, at 0:00 UTC shown in figure 2(a), and a constant  $2.4 \text{ m s}^{-1}$  wind profile, dramatically differ from their counterparts in figure 7. (a)  $x = 2$  km, (b)  $x = 3$  km, (c)  $x = 4$  km and (d)  $x = 5$  km.

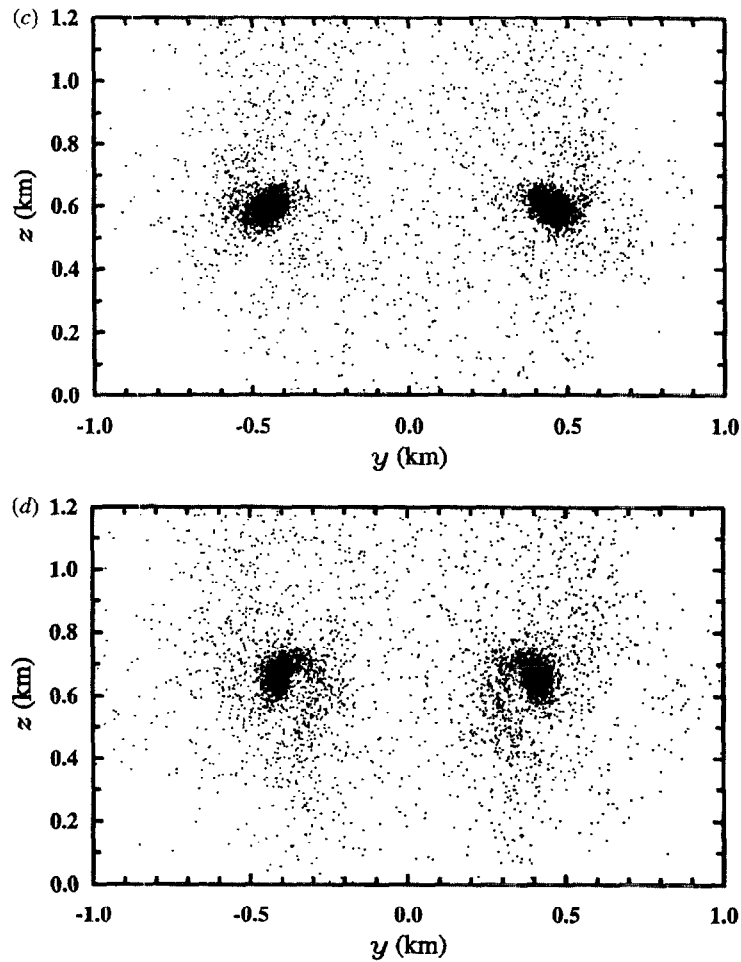
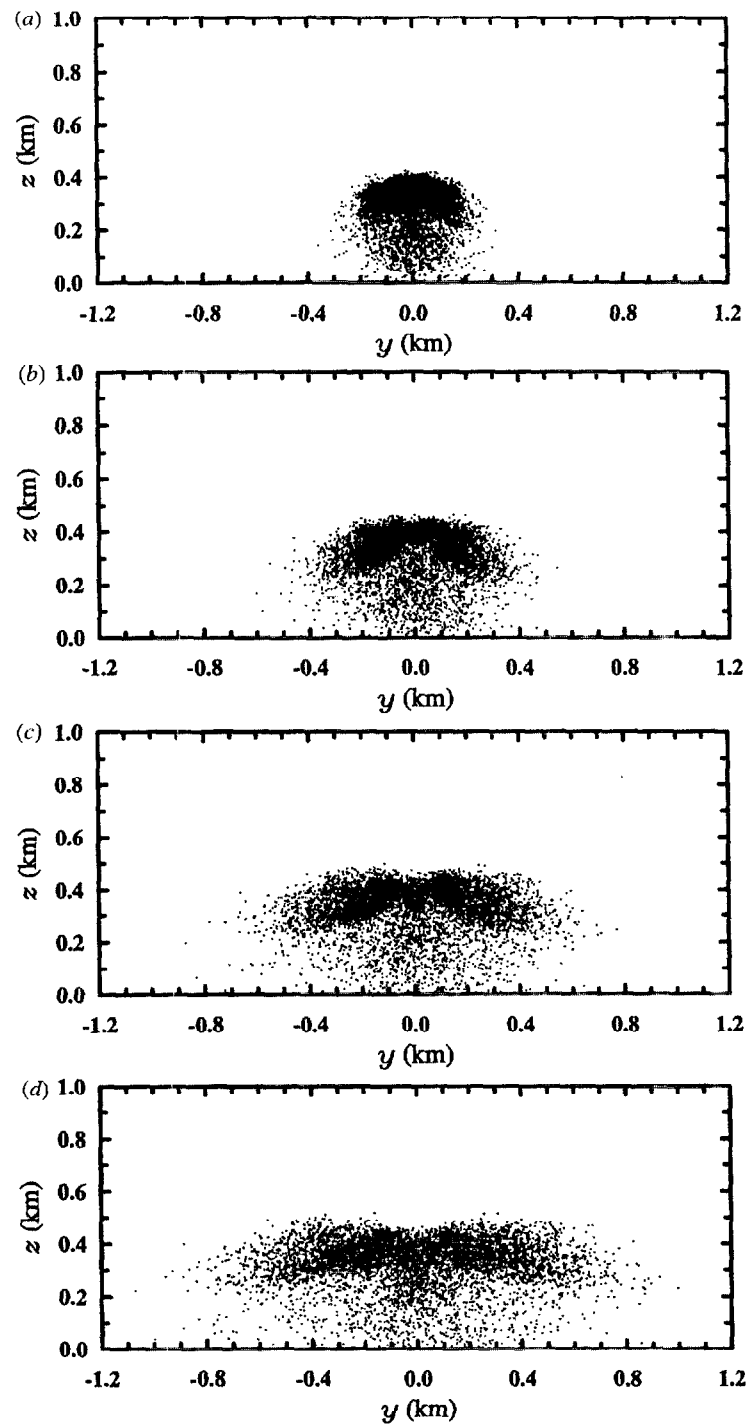


Figure 8. Continued.

also demonstrate that the model is robust enough to handle coarse profiles. In all the plots that follow, only a subset of the computational domain is shown so that the details may come out better. A  $512 \times 128$  grid is used for all calculations.

The first sounding, taken from Fairbanks, Alaska, at 12:00 universal time coordinated (UTC) on November 7 1990, is characterized by a relatively complex wind profile and a nearly linear temperature profile (see figure 1). The wind, for all its kinks, is a planar jet-like profile. The particulate distribution produced by advection through this atmosphere, as shown in figure 5, shows that the plume rose to a height of 400 m with the smoke concentrated in two regions. By  $x = 6$  km, the background atmospheric fluctuations have become the dominant dynamical force, leading to the end of the fire's influence on the particulate dynamics. If the wind in figure 1(b) is replaced by its averaged constant of  $7.2 \text{ m s}^{-1}$  and then the simulation is re-run with this value and the temperature profile in figure 1(a), the substantially different results shown in figure 6 are produced. The plume rises above 500 m and spreads more laterally as well. The fire's influence is still evident by  $x = 6$  km. The increasing wind profile in the first 400 m of figure 1(b) has suppressed the dynamics evident in figure 6 for the constant wind case.

The sounding in figure 2, taken from Anchorage, Alaska, at 0:00 UTC on October 7 1990, shows a wind profile that is reminiscent of a planar wake in standard fluid mechanics



**Figure 9.** These four cross sections at  $x = (2, 3, 4, 5)$  km of the particulate locations, generated with atmospheric mixing of intensity  $(\pm 5^\circ, \pm 5^\circ)$  and the ambient conditions for Oakland, California, on October 22 1991, at 12:00 UTC shown in figure 3, show that the increasing wind profile produces a barrier against which the smoke spreads out laterally. (a)  $x = 2$  km, (b)  $x = 3$  km, (c)  $x = 4$  km and (d)  $x = 5$  km.

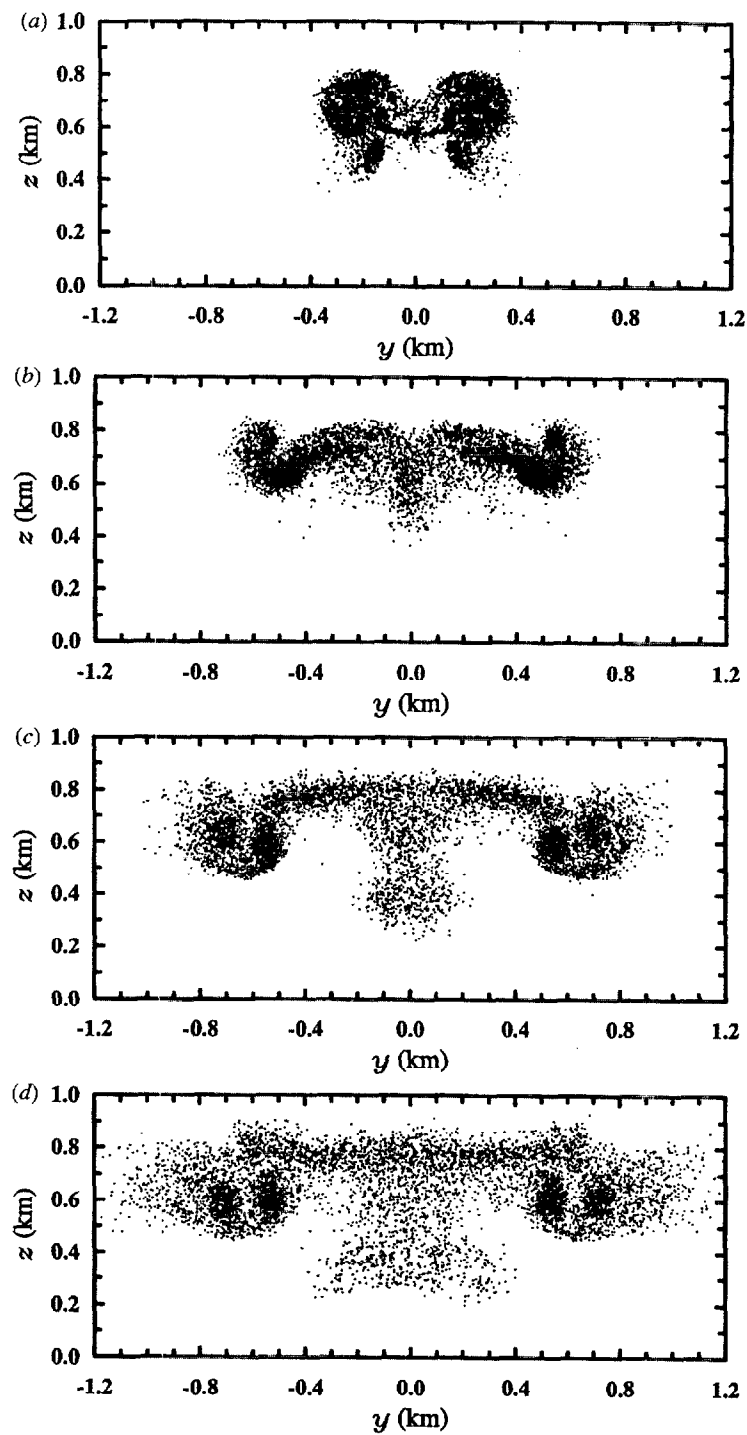


**Figure 10.** Four cross sections at  $x = (2, 3, 4, 5)$  km of the particulate locations, generated with atmospheric mixing of intensity  $(\pm 5^\circ, \pm 5^\circ)$ , the temperature sounding profile for Oakland, California, on October 22 1991, at 12:00 UTC shown in figure 3(a), and a constant  $5.1 \text{ m s}^{-1}$  wind profile, evidence the vigorous and complex dynamics that the wind profile in figure 3(b) suppressed. (a)  $x = 2$  km, (b)  $x = 3$  km, (c)  $x = 4$  km and (d)  $x = 5$  km.

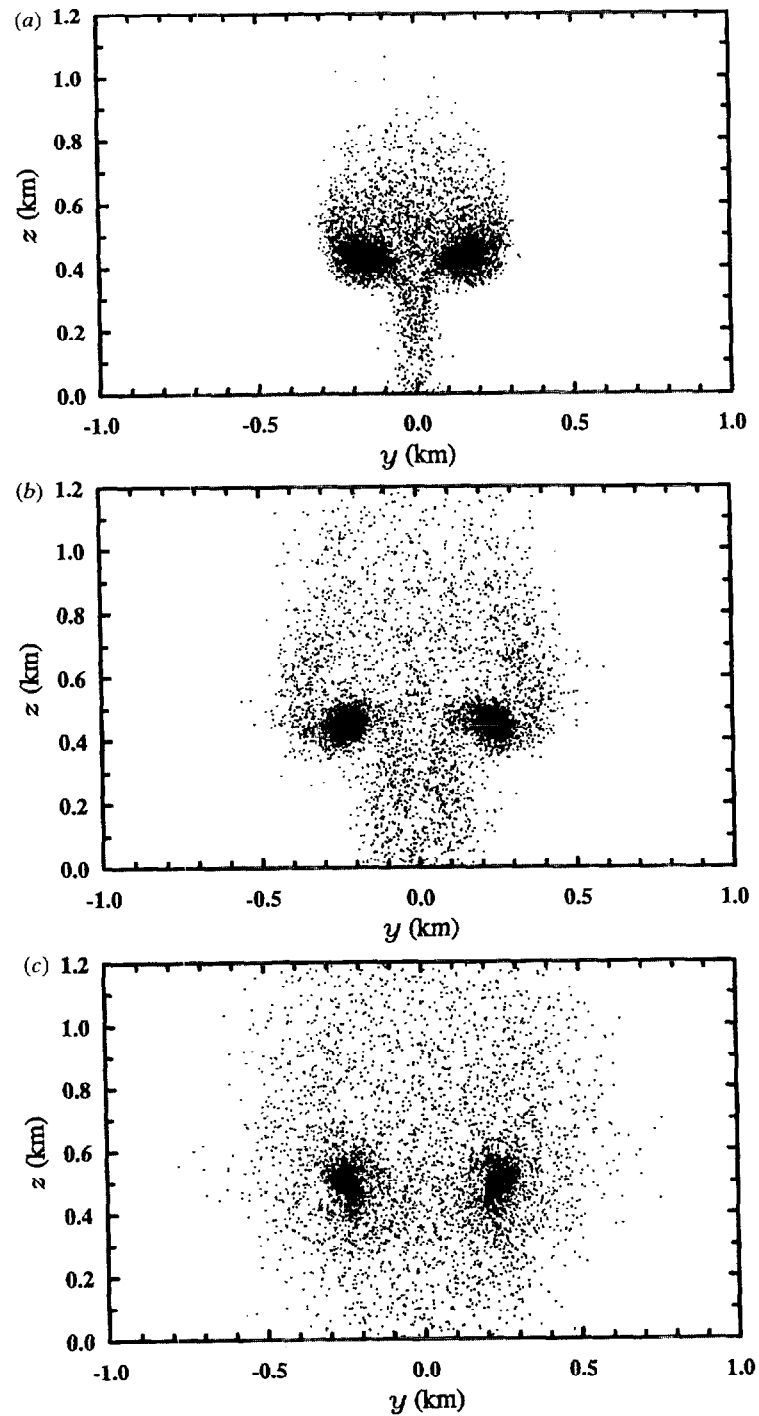


**Figure 11.** Four cross sections at  $x = (1, 2, 3, 4)$  km of the particulate locations were generated with atmospheric mixing of intensity  $(\pm 5^\circ, \pm 5^\circ)$  and the ambient conditions for Anchorage, Alaska, on October 30 1990, at 12:00 UTC shown in figure 4. (a)  $x = 1$  km, (b)  $x = 2$  km, (c)  $x = 3$  km and (d)  $x = 4$  km.

terminology. The smoke transport results, given in figure 7, show that the plume cannot climb much above 330 m, where the velocity begins to increase with height. So, as early as  $x = 4$  km,

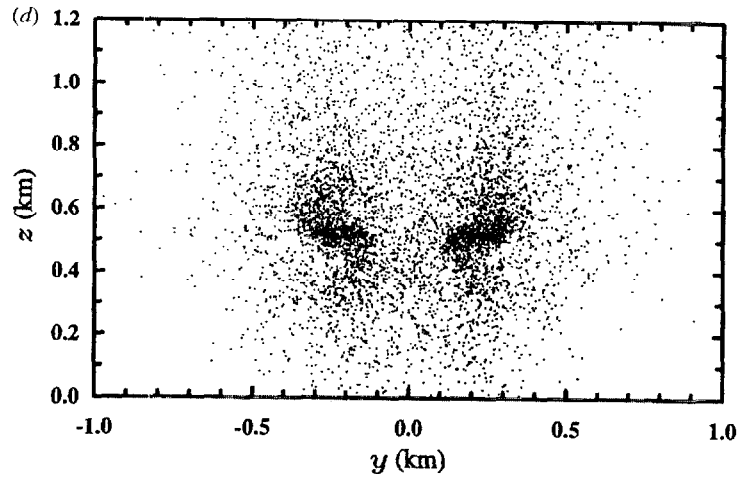
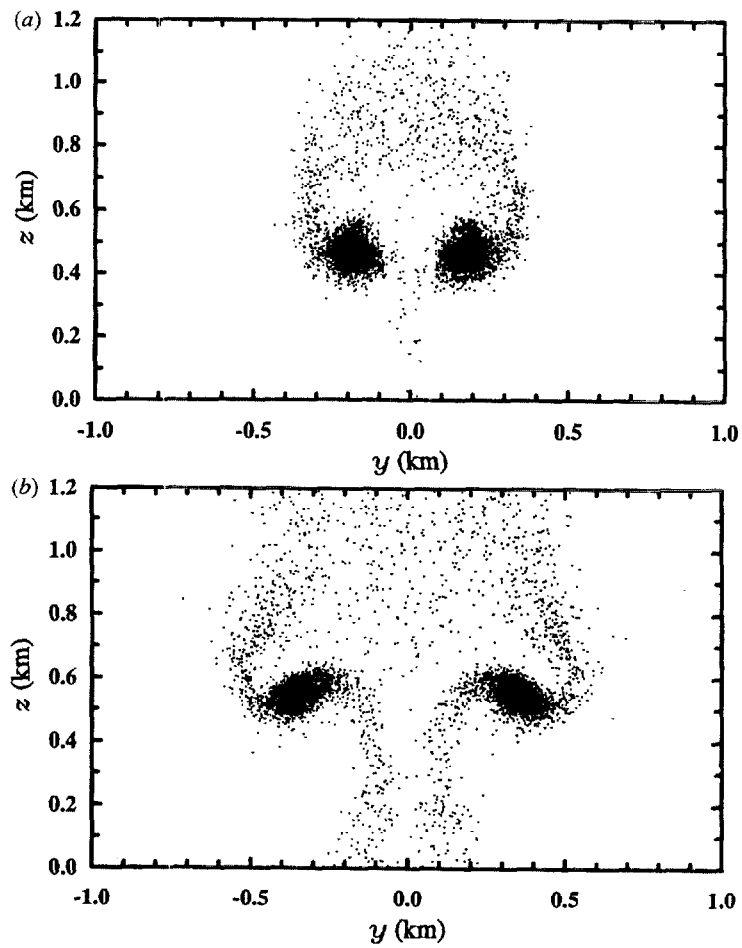


Figure 11. Continued.



**Figure 12.** Four cross sections at  $x = (1, 2, 3, 4)$  km of the particulate locations were generated with atmospheric mixing of intensity  $(\pm 5^\circ, \pm 5^\circ)$ , the temperature sounding profile for Anchorage, Alaska, on October 30 1990, at 12:00 UTC shown in figure 4(a), and a constant  $2.4 \text{ m s}^{-1}$  wind profile. (a)  $x = 1$  km, (b)  $x = 2$  km, (c)  $x = 3$  km and (d)  $x = 4$  km.

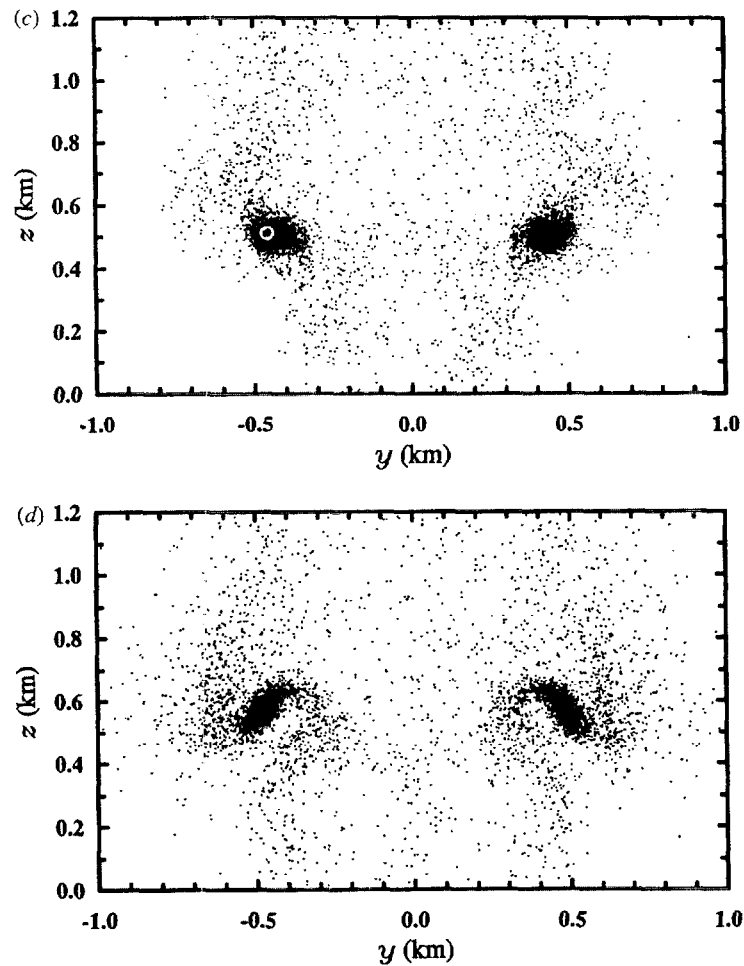


Figure 12. Continued.

the dynamics are dominated by atmospheric mixing. Now, if the wind is averaged up to the rise height of 400 m, the transport by the constant  $2.4 \text{ m s}^{-1}$  wind, shown figure 8, allows the plume to rise beyond the previous 400 m limit. At  $x = 2 \text{ km}$ , the plume has reached its stable height of about 600 m. The counter-rotating vortex pair is so strong that the jet produced in between them shoots smoke above 1.2 km. Their effect is still pronounced at  $x = 5 \text{ km}$  where the wake profile's results are much more uniformly mixed.

The wind profile for Oakland, California, at 12:00 UTC on 22 October 1991, shown in figure 3(b), is generally increasing with altitude. The temperature in figure 3(a) is almost linearly decreasing. However, the ground level temperature is the highest of all the examples presented here. The results in figure 9 show that the increasing wind profiles provides a barrier beyond which the smoke cannot rise. The particles pancake against this impediment to form an umbrella-like distribution. The dynamics for an averaged constant wind of  $5.1 \text{ m s}^{-1}$ , shown in figure 10, are quite vigorous and complex, being evident in spite of the effects of the background ambient mixing.

The last sounding addressed in this investigation, shown in figure 4, is for Anchorage, Alaska, at 12:00 UTC, on 30 October 1990. The wind is generally decreasing with height. The results in figure 11 now bear noticeable similarities to the averaged constant  $2.4 \text{ m s}^{-1}$

case in figure 12. The most striking difference is that for the constant wind case the particles spread more laterally. Furthermore, the persistence of the two regions of high concentration in figure 12 indicates that the vortices have not decayed to a level where the atmosphere dominates as is the case in figure 11. Apparently the wind shear provides an outlet for energy that would otherwise have led to regions of stronger vorticity.

## 5. Discussion

The examples shown above help to establish the conclusion that an increasing wind suppresses plume rise. Analogous behaviour can be found in the context of internal waves [13] (p 337), wherein it is shown how a vertically increasing wind profile can delay the arrival of a ray to its maximum achievable altitude. The measurements conducted by [14] found that a stable turbulent atmospheric boundary layer height was achieved below the altitude at which the wind's maximum occurs. Although the physics of these two examples have marked differences with smoke transport as presented here, they are important precedents since they show that an increasing wind profile can attenuate atmospheric phenomena. The decreasing wind, on the other hand, may destabilize the plume. Since the temperature profiles and averaged winds for these four examples differ, comparison amongst them is inappropriate. However, the four examples above demonstrate that the averaged wind profile can be a very poor substitute for the variation of wind with height where smoke transport is concerned. Hence the inclusion of the wind's variation in a fire plume model seems appropriate. In all the examples presented above, the plume behaviour cannot be described as Gaussian. Detailed simulations based on the nonlinear equations of motion would seem to be the only way to obtain the kind of results shown here. The advent of powerful, low-cost workstations together with the simplifications introduced in the model largely eliminate the computational barriers to regular use of this methodology for pollution impact assessment.

## References

- [1] Rehm G R and Baum H R 1978 The equations of motion for thermally driven, buoyant flows *J. Res. Natl Bur. Stand.* **83** 297–307
- [2] Baum H R, McGrattan K B and Rehm R G 1994 Simulation of smoke plumes from large pool fires *Proc. 25th Int. Symp. Combustion* (Pittsburgh, PA: Combustion Institute) pp 1463–9
- [3] McGrattan K B, Baum H R and Rehm R G 1996 Numerical simulation of smoke plumes from large oil fires *Atmos. Environ.* **30** 4125–36
- [4] McGrattan K B, Baum H R, Walton W D and Trelles J 1997 Smoke plume trajectory from *in situ* burning of crude oil in alaska—field experiments and modeling of complex terrain *Technical Report NISTIR 5958* (Gaithersburg, MD: National Institute of Standards and Technology)
- [5] Trelles J, McGrattan K B and Baum H R 1999 Smoke dispersion from multiple fire plumes *AIAA J.* at press
- [6] Ghoniem A F, Zhang X, Knio O M, Baum H R and Rehm R G 1993 Dispersion and deposition of smoke plumes generated from massive fires *J. Hazardous Mater.* **33** 275–93
- [7] Zhang X and Ghoniem A F 1993 A computational model for the rise and dispersion of wind-blown, buoyancy driven plumes, part 1. Neutrally-stratified atmosphere *Atmos. Environ.* **27** 2295–311
- [8] Zhang X M and Ghoniem A F 1994 A computational model for the rise and dispersion of wind-blown, buoyancy-driven plumes, part 2. Linearly stratified atmosphere *Atmos. Environ.* **28** 3005–18
- [9] Zhang X M and Ghoniem A F 1994 A computational model for the rise and dispersion of wind-blown, buoyancy-driven plumes, part 3. Penetration of atmospheric inversion *Atmos. Environ.* **28** 3019–32
- [10] Schwartz B E and Govett M 1995 A hydrostatically consistent North American radiosonde data base at the forecast systems laboratory, 1946–present *Technical Report* NOAA technical memorandum ERL FSL-4 (Boulder, CO: Forecast Systems Laboratory, National Oceanographic and Atmospheric Administration)
- [11] 1995 NOAA. *Radiosonde Data of North America 1946–1994* CD-ROM data set Forecast Systems Laboratory and the National Climatic Data Center, National Oceanographic and Atmospheric Administration

- [12] Sweet R 1990 *CRAYFISHPAK User's Guide* (Boulder, CO: Green Mountain Software)
- [13] Lighthill J 1978 *Waves in Fluids* (Cambridge: Cambridge University Press)
- [14] Kallistratova M A, Keder J, Petenko I V and Tieme N S 1991 Average wind velocity profile measurements by a sodar anemometer (Doppler sounder) in the lower troposphere under inversion and convective conditions *Izv. Akad. Nauk SSSR Fiz. Atmos. Okeana* **21** 380–3